Manuscript submitted to *Construction and Building Materials*

Hydration of C_4AF in the presence of other phases: a synchrotron X-ray powder diffraction study

A. Cuesta[a], I. Santacruz[a], S. G. Sanfélix[b], F. Fauth[c], M. A. G. Aranda[a,c], A. G. De la Torre[a,*].

[a] Departamento de Química Inorgánica, Universidad de Málaga, Campus Teatinos S/N. 29071-Málaga, Spain.

[b] Unidad Técnica de Investigación de Materiales, AIDICO, Avda. Benjamín Franklin, 17 Paterna, Valencia, Spain.

[c] ALBA-CELLS synchrotron, Carretera BP 1413, Km. 3.3, E-08290 Cerdanyola, Barcelona, Spain.

* Corresponding author. Tel.: +34952131877; fax: +34952132000.
E-mail address: *mgd@uma.es* (A.G. De la Torre)

Abstract

Hydration behaviour of C_4AF in selected experimental conditions has been determined. C_4AF has been hydrated in the absence and presence of gypsum, two polymorphs of ye'elimite and different water/solid ratios. C_4AF in the presence of water hydrates to form mainly a hydrogarnet-type phase. The crystal structure of $C_3A_{0.845}F_{0.155}H_6$ is reported from the Rietveld analysis of its synchrotron X-ray powder diffraction pattern. The hydration of C_4AF in the presence of gypsum gives AFt. However, the mixture tetracalcium aluminoferrite/gypsum/ye'elimite gives both AFt and AFm phases. C_4AF hydrated with ye'elimite in the absence of gypsum gives only AFm. Ye'elimite has inhibited tetracalcium aluminoferrite hydration.

Keywords: Hydration mechanism, Rietveld method, dissolution and crystallization kinetics, tetracalcium aluminoferrite.

1. Introduction

X-ray powder diffraction (XRPD) is very well suited for *in-situ* studies of chemical processes involving crystalline materials [1,2]. During the last years, it has been reported quantitative phase analysis of cements, clinkers and supplementary cementitious materials by combining XRPD and Rietveld methodology [3-6]. More recently, this procedure has been expanded to hydrated cementitious systems [1,7] and in some of these studies, the non diffracting fraction was also determined [8-10], although a more precise term was coined: Amorphous and Crystalline not-quantified content (ACn) [11]. Furthermore, the use of intense monochromatic X-rays, such as synchrotron X-rays, coupled with a fast X-ray detection system permits high-resolution time-resolved diffraction experiments allowing *in-situ* measurements during the hydration process of cements [1,12,13].

The tetracalcium aluminoferrite phase, C_4AF in cement nomenclature, also known as brownmillerite, is the major iron-containing phase in Ordinary Portland Cement (OPC) and is also present in iron rich belite calcium sulfoaluminate cements [14-15]. This phase has been deeply studied [16–19] and for this reason, their crystal structures and chemical compositions are currently known, including the structural variations which have placed in the $Ca_2(Fe_{2-y}Al_y)O_5$ series [20], where y can oscillate from 0 to about 1.33 [19] in high iron content cements. In Portland cements this phase is supposed to have an ideal composition with y=1. However, it has been reported that other elements could be also present in the composition of the C_4AF phase and for this reason the A/F ratio is not exactly unity [21].

In the absence of any other phases, the hydration of C_4AF is similar to the hydration of C_3A, in which a C-A-H gel first coats the C_3A grains. This gel presents metastable hexagonal C-A-H plates that finally convert to the stable cubic hydrate C_3AH_6 [22-24]. However, the hydration products are (quite often) assumed to incorporate some iron in the case of the tetracalcium aluminoferrite phase [25-29]. Firstly, in the hydration of tetracalcium aluminoferrite with water a metastable type-gel C-(A,F)-H [28] is formed and with the time this gel converts to a hydrogarnet phase, also known as

katoite, $C_3(A,F)H_6$ [28], with an Al/(Al + Fe) ratio of about 0.4. However, other authors [25,30,31] stated that solid solution between C_3AH_6 and C_3FH_6 is not formed.

The exact Al/Fe ratios of the hydrogarnets are as yet under debate but it is generally accepted that the Al/Fe ratio of the crystalline products is greater than in C_4AF itself [32].

The hydration of C_4AF [28] could be written as:

$$C_4AF + 10H \rightarrow C_3AH_6 + FH_3 + CH \quad (1)$$

where FH_3 indicates a hydrated amorphous Fe-containing gel. If the case that Fe is incorporated into the hydrogarnet product, then the reaction could be expressed as:

$$C_4AF + 10H \rightarrow \tfrac{4}{3}C_3(A_{0.75}F_{0.25})H_6 + \tfrac{2}{3}FH_3 \quad (2)$$

When calcium sulfates are added, the direct hydration of C_4AF to $C_3(A,F)H_6$ is inhibited. Consequently, ettringite is the common hydration product observed in this case. There are some theories about the mechanism governing the retardation process. However, the formation of hydroxy-AFm gel surrounding C_4AF particles which yields to ettringite crystallization centers is the most likely mechanism [29].

In the presence of a source of sulfate the reaction could be formulated as [28]:

$$C_4AF + 3C\bar{S}H_2 + 30H \rightarrow C_6A\bar{S}_3H_{32} + CH + FH_3 \quad (3)$$

where $C_6A\bar{S}_3H_{32}$ denotes ettringite (also known as AFt). Again, iron may be incorporated in the ettringite structure as detailed by [26] according to reaction (3.1):

$$C_4AF + 4C\bar{S}H_2 + \tfrac{106}{3}H \rightarrow \tfrac{4}{3}C_6(A_{0.75}F_{0.25})\bar{S}_3H_{31} + \tfrac{2}{3}FH_3 \quad (3.1)$$

where $C_6(A_{0.75}F_{0.25})\bar{S}_3H_{32}$ stands for iron-bearing AFt.

Successively, ettringite can decompose to form an AFm monosulfoaluminate hydrate in the presence of C_4AF as stated next:

$$C_6A\bar{S}_3H_{32} + C_4AF \rightarrow 2C_4A\bar{S}H_n + C\bar{S}H_2 + (26 - 2n)H + FH_3 + CH \quad (4)$$

If there is any amount of C_4AF, this could react with gypsum to form AFm ($C_4A\bar{S}H_n$), then the reaction could be expressed as:

$$C_4AF + C\bar{S}H_2 + (n + 2)H \rightarrow C_4A\bar{S}H_n + FH_3 + CH \quad (5)$$

Moreover, it has been reported [28] that a partial series of solid solutions can be formed between C_3AH_6 and C_3FH_6; accordingly the previous equations could be also expressed in terms of $C_x(A,F)_yH_z$ or $C_x(A,F)_y\bar{S}_wH_z$.

The main purpose of the present work has been to study the hydration of C_4AF phase in different environments: in the presence and absence of gypsum and in the presence of both polymorphs of ye'elimite, stoichiometric (orthorhombic) and solid solution (pseudo-cubic). The interest of studying these systems as simple mixtures is to better understand the hydration mechanisms of new eco-cements based on calcium sulfoaluminate, which contains different polymorphs of ye'elimite with C_4AF [12, 14]. In order to do so, synchrotron XRPD (SXRPD) and Rietveld methodology are employed. The advantage of using high energy radiation is mainly the minimization of microabsorption effects. Kinetics of hydration have been established and correlated to calorimetric data. Scanning electron microscopy (SEM) has been also done to corroborate the results. Moreover, high-resolution SXRPD and transmission electron microscopy (TEM) were used to refine the crystal structure of one of the hydrated crystalline phases, $C_3(A,F)H_6$.

2. Experimental Section

2.1. Sample preparation.

Tetracalcium aluminoferrite (C_4AF) was prepared by mixing suitable amounts of $CaCO_3$ (99.95%, Alfa Aesar), Al_2O_3 (99.997%, Alfa Aesar) and Fe_2O_3 (99.945%, Alfa Aesar), to obtain approximately 50 g of sample with targeted chemical formula of Ca_2AlFeO_5, i.e. x=1. The raw mixture was ground for 5 minutes and heated at 1000ºC for 4 hours (heating rate of 10 ºC/min). After that, the powder was ground for 45 min in a Micro-deval machine with a cylinder container and steel balls and was pelletized (600 mm diameter and 1000 MPa). Finally, the pellets were

heated at 1350ºC for 4 hours (heating rate of 10 ºC/min) followed by quenching from high temperature with an air flow.

Moreover, stoichiometric (st-) $Ca_4[Al_6O_{12}]SO_4$ and solid solution (ss-) $Ca_{3.8}Na_{0.2}Al_{5.6}Fe_{0.2}Si_{0.2}O_{12}SO_4$ ye'elimites has been used for this study. Ye'elimite polymorphs were prepared as previously reported [33, 34].

C_4AF was mixed, in some cases, with gypsum (g), stoichiometric (st-) or solid solution (ss-) ye'elimite. Table 1 reports paste mix proportions, including water/solid (w/s) ratios. The gypsum used for the hydration studies was that marketed by BELITH S.P.R.L. (Belgium).

For this study, *in-situ* SXRPD experimental set up was employed. All the anhydrous mixtures were mixed with 15 wt% of SiO_2 (99.56%, ABCR) as an internal standard [13, 35] and SXRPD data were collected to obtain the initial phase assemblage (t_0). This standard presents an amorphous content of 12.7(1) wt% which was determined by the external standard method [36]. Moreover, it is important to bear in mind that in the reported water/solid ratio, the amount of internal standard is not taken into account. Pastes were *ex-situ* prepared and immediately loaded into glass capillaries of 0.5 mm of diameter with a syringe. The capillaries were sealed with grease to avoid any water loss.

2.2. Synchrotron X-ray powder diffraction (SXRPD).

SXRPD patterns were collected at room temperature in Debye-Scherrer (transmission) mode using the high-resolution X-ray powder diffraction beamline of ALBA synchrotron (Barcelona, Spain) [37]. The wavelength, 0.61975(1) Å, was selected with a double-crystal Si (111) monochromator and determined from Si640d NIST standard (a=5.43123 Å). The diffractometer is equipped with a MYTHEN detector especially suited for time-resolved experiments. The capillaries were rotated during data collection to improve diffracting particle statistics and the synchrotron beam was focused in the detector to improve the powder diffraction peak shapes. The data acquisition time was ~15 min per pattern to attain very good signal-to-noise ratio over the angular range 1-35º (2θ).

The diffractometer is also equipped with a detector system based on crystal analyzers in the diffracted beam especially suited for extremely high-resolution experiments giving also a very flat background. One of the samples was measured with this detector in a capillary of 0.5 mm of diameter that was rotated at 400 rpm during data collection to improve diffracting particle statistics. The data acquisition time was very long, ~4 hours, to attain a very good signal-to-noise ratio over the recorded wide angular range 1-45º (2θ), to perform the structural study of a crystalline hydrate sample, see below.

2.3. SXRPD data analysis.

Raw SXRPD patterns were normalized taking into account the decay of X-ray beam flux with time. Patterns were analysed by using the Rietveld methodology as implemented in the GSAS software package [38], in order to obtain Rietveld quantitative phase analysis (RQPA). The refined overall parameters were background coefficients, cell parameters, zero-shift error, peak shape parameters, and phase scale factors. Powder diffraction peak shapes were fitted by using the pseudo-Voigt function [39]. The ACn contents were determined by internal standard methodology [35] from SXRPD data as detailed previously [13]. For the structural analysis, atomic parameters, in addition to the overall parameters, were also optimised.

2.4. Isothermal calorimetry.

The isothermal calorimetric study was performed in an eight channel Thermal Activity Monitor (TAM) instrument using glass ampoules. Some pastes were selected and were prepared *ex-situ* by mixing ~6 g of each sample with the appropriated water amount. Then, the pastes were immediately introduced in the calorimeter. A stabilization period of 45 minutes was needed to start the measurements. The heat flow was collected up to 2 days at 20ºC.

2.5. Scanning electron microscopy (SEM) and transmission electron microscopy (TEM) studies.

Prior to SEM observation, the hydration of selected samples was stopped by immersing them in isopropanol for 3 days and then heated at 40 ºC for 24 h. Samples suitable for the SEM characterization were prepared in cylinders following the methodology previously reported [13].

Microscopic characterization of samples was performed in a JEOL JSM-6490LV. Samples were impregnated with low viscosity resin and polished down to 1 μm using diamond spray and further sputtered with graphite. Energy dispersive spectroscopy (EDS) measurements were carried out with the OXFORD INCA Energy 350 attachment. The voltage used was 20 kV and the working distance was around 10 mm.

Moreover, the fracture cross-sections of some pastes after 48 hours of hydration were also observed by SEM in a JEOL-JSM-840. These samples were gold sputtered.

Finally, TEM studies were done in a Philips CM-200 for some particles of a hydrated sample (without any thermal/chemical treatment to stop hydration), with microanalysis performed with the EDAX Génesis-4000 attachment.

2.6. Thermal analysis.

Differential thermal analysis (DTA) and thermogravimetric (TGA) measurements were performed in a SDT-Q600 analyzer from TA instruments (New Castle, DE) in non-stopped hydration samples. The temperature was varied from RT to 1000ºC at a heating rate of 10 ºC/min. Measurements were carried out in open platinum crucibles under air flow.

3. Results and discussions.

Initial C_4AF characterization. The C_4AF sample was studied by SXRPD and the Rietveld method. For this synthesis, the only additional phase was C_3A, 1.94(6) wt%. The derived unit cell parameters for C_4AF, from SXRPD, were: a=5.56638(4)Å, b=14.5227(1)Å, c=5.34835(4)Å and V=432.354(8) $Å^3$. As the quality of the SXRPD was very high, we could optimize the Fe/Al ratio in the octahedral and tetrahedral sites (constrained to an overall Fe/Al ratio of 1.00). The resulting value was 0.746(2) of Fe occupancy at the octahedral site and therefore 0.254(2) of Fe occupancy at

the tetrahedral site. We are aware that different cooling rates could change Fe/Al distributions at these sites but to study the possible consequences of this variation on the hydration properties of C_4AF is out of the scope of the present work.

3.1. Hydration of C_4AF.

Initially, the hydration behaviour of just C_4AF was studied. The w/s ratio used was 0.8, see Table 1. *C_4AF_0.8* sample has been characterized up to 5.5 hours by *in-situ* SXRPD with internal standard methodology for determining the ACn content. Time-resolved SXRPD was employed to track the dissolution of the anhydrous phases followed by the crystallization of the different hydrated phases. Table 2 shows the phase assemblages at different ages. In agreement with reaction (2), $C_3(A,F)H_6$ crystallized, and during the first hours some C_2AH_8 was also formed. It has been reported that C_2AH_8 phase is formed after 5 minutes from hydration and then it abruptly converts into $C_3(A,F)H_6$ [28]. In this study, the first pattern was taken at 1 hour, consequently big amounts of C_2AH_8 phase were not expected and $C_3(A,F)H_6$ is the main phase after 5.5 hours of hydration. Moreover, the small amount of C_3A in this sample does not affect the hydration products as only hydrogarnet with iron was observed at all the hydration times. The hydrogarnet type phase present in all the patterns presented systematic peak shifts, indicating the formation of the solid solution $C_3(A,F)H_6$ in agreement with [28] and in contrary with results presented in [25,30,31].

The first column in Table 2 gives t_0 values obtained from the SXRPD pattern of the anhydrous sample renormalized with theoretical free water, FW. Remaining values obtained from internal standard method encompass not only ACn but also FW (not chemically bound water) and are expressed as a single value in Table 2.

ACn and FW are expressed as a single value due to the inability of the internal standard methodology to distinguish between different not-diffracting phases. It can be observed that these values slightly diminished with time. This is mainly due to the precipitation of a crystalline phase, $C_3(A,F)H_6$, which is consuming free water.

C_4AF was also hydrated with w/s ratio of 1.0, in order to accelerate the reaction and with the aim of obtaining $C_3(A,F)H_6$ as single crystalline phase after 24 hours of hydration according to reaction (2). The w/s ratio and the rotation of the capillary during measurement may be the responsibles of the fast hydration kinetics of C_4AF. As the hydrated paste in these conditions contained a single crystalline phase, SXRPD has been used to obtain a revised crystal structure of $C_3(A,F)H_6$.

3.1.1. Structural study of $C_3(A,F)H_6$.

High-resolution SXRPD was employed to study the crystal structure of crystalline $C_3(A,F)H_6$ prepared by direct hydration of C_4AF. We have used the structural description reported by Lager et al. [40], with space group $Ia\bar{3}d$, as a starting model for the structural Rietveld refinement. However, this structure does not include iron. The initial amount of iron, 0.20, was chosen using data reported in Table 6.4 in Taylor et al. [21] by interpolating the refined unit cell parameter, *a*.

The structural description reported by Lager et al. [40] for C_3AH_6 has three crystallographically independent sites: one Ca and one Al (or Fe, in our case) in special positions (24c and *16a* respectively); and one oxygen in general position (*96h*). Once the overall parameters were optimized, the atomic parameters were refined, including the atomic positional coordinates, isotropic atomic displacement parameters (Uiso) and occupation factors for Al and Fe. In the final cycle, the obtained disagreement factors were R_{WP}=8.1% and R_F=4.8% and the determined formula was $C_3A_{0.845}F_{0.155}H_6$. Figure 1 shows the final SXRPD Rietveld plot using the optimized structure. The final refined unit cell parameter and the cell volume were a=12.60315(4) Å and 2001.88(2) $Å^3$, respectively. The refined atomic parameters for this sample, measured at room temperature, are provided in Table S1 as supplementary material. The corresponding CIF file has also been deposited. According to the stoichiometry determined by SXRPD Rietveld analysis an alternative to reaction (2) could be proposed:

$$C_4AF + 10H \rightarrow C_3A_{0.845}Fe_{0.155}H_6 + 0.845FH_3 + 0.155AH_3 + CH$$

TEM, combined with EDS was used in this sample to quantify the amount of iron in this hydrogarnet-type structure. Some particles of $C_3(A,F)H_6$ were analyzed and the obtained average

composition matched relatively well with that determined by the Rietveld methodology, see Table 3; except for the iron content which is larger in TEM-EDS results. Rietveld methodology gives an average composition as the result of analyzing a representative sample. However, TEM-EDS analysis results are less representative as just a limited number of particles (six particles) are inspected. Another likely explanation of this discrepancy is the possible coating of $C_3(A,F)H_6$ particles with an iron reach gel which is not computed in the SXRPD analysis but it affects the TEM measurements. In any case, the most important result of this part of the study is that the incorporation of iron in C_3AH_6 is possible and this phase is sufficiently stable. Moreover, as previously reported [32], the Al/Fe ratio is higher than in the anhydrous phase. As the iron content of the product is lower than that of C_4AF the fate of iron is still contentious. It is assumed that iron also goes to an amorphous iron rich gel, like the hydrated alumina-type gel, as hydration proceeds [29, 32]. The quantification of the ACn content of this sample by the internal standard method gave 58.8(2) wt% which includes free water and an iron-rich amorphous gel. This value is in agreement with other samples studied in this work, see below. Figure S1, provided as supplementary material, shows TEM micrograph of $C_3A_{0.845}F_{0.155}H_6$ sample showing the expected cubic morphology (view along [111] axis).

3.2. Hydration of C_4AF with gypsum

The effect of the gypsum on the hydration mechanism of C_4AF has also been studied. C_4AF was mixed with gypsum using the same proportion as Meller et al. [28], and with a w/s ratio of 1.0 (*$C_4AF\_g\_1.0$*), see Table 1 and with the internal standard as detailed in the experimental section. Table 4 shows the RQPA obtained by analysing *in-situ* SXRPD patterns up to 48 hours of hydration, as in Table 2 and Figure 2 shows raw SXRPD patterns as a function of hydration time. In the first stage of the hydration, AFm-type phases were not identified and consequently only reaction (3) or (3.1) to form AFt took place. However, portlandite (CH) was not detected by XRPD. In addition, the presence or absence of this phase was tested by DTA-TGA and no signal from the decomposition of portlandite was found. Figure S2, provided as supplementary material, shows the

DTA-TGA curves for this sample at 2 days of hydration, signals found until 170ºC correspond to free water, AFm and AFt phases [41]. Later, when gypsum was totally consumed, the AFt started to decompose to yield an AFm-type phase, according to reactions (4) or (5). The extension of both reactions is not an easy task but this (partial) conversion from AFt to AFm, reactions (4) and (5), have been studied and discussed previously by other authors [28] and our results are in full agreement with the previous report. It is important to bear in mind that the quantification of AFm-type phases presents two important problems: i) broad diffraction peaks due to both poor crystallinity and highly disorder structures and ii) lack of structural descriptions for some of these phases. Thereby, the crystal structure reported for $C_4A\bar{S}H_{12}$ by Allmann [42] has been used here to quantify the AFm-type phases by adjusting c-values, as previously reported [13]. The obtained c-value [28.63(1) Å] indicates the crystallization of $C_4A\bar{S}H_{14}$ AFm [21] in this sample.

The time evolution of ACn and FW contents for this sample are also reported in Table 4. It can be observed that these values slightly diminished with time until 16 hours. This is mainly due to the presence of larger amounts of ettringite and the absence of AFm-type phases. However, the opposite behaviour is observed from 16 hours due to the precipitation of AFm and the release of free water according to reaction (4) or amorphous iron and calcium hydroxides as stated in reaction (5). We highlight that the conversion of AFt to AFm should increase the amorphous content and this is clearly reported in Table 4.

Calorimetric data shows a broad signal between 20 and 30 hours of hydration associated to dissolution and precipitation processes, see Figure S3 in supplementary material. This could be related to the AFm formation which occurs close to that time. However, the formation of AFt seems to occur very fast and the calorimetric signal due to its formation/precipitation cannot be recorded as a consequence of the 45 minutes of stabilization needed in the experimental set up used. The total heat evolved after 48 h of hydration was also given in Table 1.

A SEM-EDS study was performed for the sample hydrated up to 48 h in order to unravel if AFt and AFm phases had incorporated iron in their crystal structures. It is shown in Figure 3a that those

particles with needle and laminar shapes (upper SEM photograph) presented similar compositions to AFt and AFm, respectively, and they contain small quantities of iron. Moreover, another proof to check if AFm and AFt are incorporating iron is by testing their lattice parameters. For instance, this AFm phase presents a cell parameter of a=6.100(8) Å and c=28.63(1) Å, while the AFm formed in the direct hydration of ye'elimite [13] gave an average lattice parameter of a=5.754(1) Å and c=28.66(2) Å. The higher value of a, which is related to the brucite-type layer $[Ca_2Al_{(1-x)}Fe_x(OH)_6 \cdot 2H_2O]^+$ may indicate the incorporation of iron in the structure. We can speculate that mechanism of hydration to form AFm phases has followed the reaction:

$$C_4AF + C\bar{S}H_2 + (n+2)H \rightarrow C_4(A_{0.75}F_{0.25})\bar{S}H_n + + \tfrac{3}{4}FH_3 + CH + \tfrac{1}{4}AH_3$$

The stoichiometry of iron-bearing AFm has been proposed according to [26].

In the case of AFt, due to its symmetry the comparison of volume is more illustrative. The AFt volume of this sample is 2351.4(6) $Å^3$ and for the sample of pure ye'elimite [13] was 2346.9(4) $Å^3$. Again, the observed volume of AFt formed in this sample is higher due to the fact that iron is replacing aluminium in the structure. This fact may indicate that reaction (3.1) is the most likely one. Moreover, these results also show that there are some bright particles observed by SEM with very high amount of iron which have been assigned as iron-bearing ACn phases. This last result indicates that reaction (5) is taking place although it does not rule out that reaction (4) is also occurring. A fracture cross-section of sample was also studied by SEM, Figure S4a provided as supplementary material. Small needle and laminar shape particles are clearly observed due to AFt and AFm phases respectively.

3.3. Hydration of C_4AF with two different polymorphs of ye'elimite.

3.3.1. Role of ye'elimite polymorphism. The role of ye'elimite polymorphism in the hydration of C_4AF has also been investigated. Mixtures containing stoichiometric (st-) [33], or solid solution (ss-) [34] ye'elimites, with tetracalcium aluminoferrite and with or without gypsum were prepared, see Table 1. These proportions were chosen to simulate previously reported laboratory BCSA

cements [3] excluding belite phases, in order to study the hydration mechanisms of high soluble phases.

Firstly, st-ye'elimite, C_4AF and gypsum were mixed with a water/solid ratio of 1.0 (*C_4AF_st-$C_4A_3\bar{S}$_g_1.0*). This paste has been studied at early ages, up to 46 hours. Table S2, provided as supplementary material, shows the RQPA obtained by SXRPD of this mixture as in Table 2 and Figure 4a shows raw SXRPD patterns as a function of time, with peaks due to a given phase labelled. Initially, only reaction of st-ye'elimite with gypsum to form AFt took place. Secondly, when gypsum was totally consumed, AFt started to decompose and AFm phase started to crystallize. The formation of AFm was favoured not only from ye'elimite reaction but also likely from AFt dissolution. However, C_4AF hydration seemed to be slightly delayed by the presence of st-ye'elimite as it started to significantly dissolve after 5 hours. The time evolution of ACn and FW contents has the same behaviour as described above for *C_4AF_g_1.0*. It can be observed that these values slightly diminished with time during the crystallization of AFt and it increased at the time that AFm started to appear.

Moreover, the full phase content evolution is displayed in Figure 5a, where calorimetric data are also included. The calorimetric curve shows a double maximum between 4 and 12 hours which agrees well with the data obtained by SXRPD. The first peak may be correlated with the ye'elimite dissolution and the second one with the C_4AF dissolution. The calorimetric signal could be also related with AFm formation.

Secondly, ss-ye'elimite was also used in the sample labelled as *C_4AF_ss-$C_4A_3\bar{S}$_g_1.0*, see Table 1. As previously reported, solid solution ye'elimite had different hydration behaviour than stoichiometric ye'elimite [13]. Figure 4b shows raw SXRPD patterns as a function of time, with peaks due to a given phase labelled. In addition, Table S3, provided as supplementary material, shows the phase assemblages as a function of time up to 46 hours of hydration for this sample and Figure 5b gives the phase content evolution and calorimetric data. Here, ss-ye'elimite started to quickly consume and AFt precipitated/formed at early stage. However, although ss-ye'elimite and

gypsum were completely dissolved, C_4AF hydration was strongly slowed down (arrow in Figure 4), as it started to form AFm only after 28 hours of hydration. AFt content reached a maximum content at 28 hours under the studied experimental conditions. Moreover, the ACn and FW evolution was in agreement with the crystalline phase evolution (as reported above), diminishing with time during the crystallization of AFt and increasing at the time that AFm started to appear. Figure 5b shows a signal in the calorimetric curve between 4 and 18 hours. The signal could be related with the formation of AFt which is increasing until 21 hours as we can see in the RQPA. This signal is broader than for the st-ye'elimite due to the slower formation of AFt. The total heat evolved at 48 hours is also given in Table 1, being higher than that of st-ye'elimite, corroborating that AFt formation takes place in a broader period of time.

Inspecting Figure 4, 5 and Tables S2 and S3 in supplementary material, it is highlighted that the main difference after 46 hours is that the sample with ss-ye'elimite yielded much larger relative amounts of AFt as we reported in a previous publication [13]. The hydration behaviour for *C_4AF_ss-$C_4A_3\bar{S}$_g_1.0* is totally different to the other samples. Moreover, it may seem that the dissolution of C_4AF has been partly inhibited and this is the reason why only small quantities of AFm were quantified here. One hypothesis for this behaviour could be that the hydration of ye'elimite, which is much faster, consumes a significant amount of water and at the same time its hydration products fill the pores before C_4AF starts to react. For this reason, the driving force for C_4AF to hydrate will be quite low.

A SEM-EDS study was also performed for *C_4AF_st-$C_4A_3\bar{S}$_g_1.0* and *C_4AF_ss-$C_4A_3\bar{S}$_g_1.0* pastes at 48 hours of hydration. It can be observed in Figure 3b that most particles, with similar compositions to AFt and AFm, do not contain significant amounts of iron. Bright particles with high iron contents were also observed in these samples and also a dark gray background with a very large Al/Ca ratio which may be related to aluminium-rich ACn phases [43]. Moreover, Figure S4b, provided as supplementary material, shows a micrograph of the fracture cross-section of *C_4AF_ss-$C_4A_3\bar{S}$_g_1.0* paste after 48 h of hydration, where large needle shape particles due to AFt are

observed. The lattice parameters of AFm and AFt were also checked. The average lattice parameters obtained for the AFm formed in these samples are a=5.758(4) Å and c=28.66(3) Å and the volume of AFt was 2348.2(4) $Å^3$. These values are quite similar to that obtained in the hydration of pure ye'elimite without C_4AF [13] given above. This may be due to the fact that the incorporation of iron is not taking place in these samples.

3.3.2. Role of w/s ratio. The sample which contains st-ye'elimite, tetracalcium aluminoferrite and gypsum was hydrated with 0.7 and 1.3 w/s ratios up to 12 hours. Tables 5 and 6 show the phase assemblages with time for both mixtures. It is well known that higher amounts of water enhance ye'elimite reactivity [13, 41] as well as the other cementitious systems (OPC, Calcium Aluminate Cements, etc). Figure S5, provided as supplementary material, confirms this behaviour showing the degree of reaction of ye'elimite for these samples. Moreover, in the case of *C_4AF_st-$C_4A_3\bar{S}$_g_0.7*, the main hydration product was AFt, within 12 hours in contrast with *C_4AF_st-$C_4A_3\bar{S}$_g_1.0* and *C_4AF_st-$C_4A_3\bar{S}$_g_1.3* where there was a competition between AFm and AFt. That indicates that higher amounts of water favour the formation of AFm, in agreement with a previous report [13]. Figure 6a and 6b shows Rietveld plots for *C_4AF_st-$C_4A_3\bar{S}$_g_0.7* and *C_4AF_st-$C_4A_3\bar{S}$_g_1.3*, respectively, at 12 hours of hydration. This Figure illustrates the small amount of AFm with respect to AFt for *C_4AF_st-$C_4A_3\bar{S}$_g_0.7*, see Figure 6a. However, for *C_4AF_st-$C_4A_3\bar{S}$_g_1.3*, the presence of both hydrates phases, AFt and AFm, is clearly seen (Figure 6b).

3.3.3. Hydration of C_4AF and st-ye'elimite in the absence of gypsum. Finally, *C_4AF_st-$C_4A_3\bar{S}$*_1.0 sample, see Table 1 was studied. The w/s ratio was 1.0. Table 7 shows the phase assemblage as a function of time up to 20 h. The main difference when compared to the sample with gypsum, *C_4AF_st-$C_4A_3\bar{S}$*_g_1.0, is that AFm was the only hydration product and AFt was not observed at any time. Moreover, ACn and FW contents were more or less constant with time due to that the consumption of water was being compensated by the formation of AFm, which also develops a high amorphous content.

Finally, we would like to highlight that we have shown in a previous work that st-ye'elimite hydration (without gypsum) gives AFt (and also some amounts of AFm which depends upon the water/ye'elimite ratio) [13]. AFt is formed because ye'elimite dissolution is also releasing sulfate anions to the water in the porous microstructure [13]. Now, when we compared these results with those shown in Table 7, it is clear that the presence of C_4AF has inhibited the formation of AFt from ye'elimite. Moreover, the hydration of tetracalcium aluminoferrite has also been inhibited by the presence of ye'elimite, see Table 7, as it has not significantly reacted after 20 hours.

4. Conclusions

This work reports a comprehensive hydration study of C_4AF. Several parameters have been tested to unravel their effects on tetracalcium aluminoferrite hydration behaviour, such as the presence of different sulfate sources (gypsum or calcium sulfoaluminate phase) and the water/solid ratio.

C_4AF in the presence of water hydrates to form mainly a hydrogarnet-type phase $C_3(A,F)H_6$. The hydration of C_4AF with w/s ratio of 1.0 yielded to $C_3A_{0.84}F_{0.16}H_6$ as single crystalline phase. Its crystal structure has been analyzed by the Rietveld method and reported here.

The presence of sulfates strongly modifies tetracalcium aluminoferrite hydration behavior. The hydration of C_4AF in the presence of gypsum gives AFt and amorphous aluminum hydroxide and once gypsum is completely dissolved crystalline AFm starts to precipitate jointly with more amorphous phase(s). SEM-EDS studies showed that both AFt and AFm phases contain iron.

The hydration of two different polymorphs of ye'elimite with tetracalcium aluminoferrite in the presence of gypsum has also been studied. The mixture of tetracalcium aluminoferrite, gypsum and stoichiometric ye'elimite (which is orthorhombic) gives a mixture of AFt and AFm phases. However, C_4AF hydration is slightly slowed down and moreover, these hydration products did not contain iron in their structures as determined by SEM-EDS. The retarder effect of ye'elimite over C_4AF hydration was much stronger with solid solution ye'elimite (which is pseudocubic), and consequently AFt was the main hydration phase.

The effect of w/s ratio has also been studied in the sample containing tetracalcium aluminoferrite, gypsum and stoichiometric ye'elimite. Results indicate that higher amounts of water favour the formation of AFm.

Finally, C_4AF hydrated with ye'elimite in the absence of gypsum gives AFm as the unique hydration product. Consequently, it has been demonstrated that gypsum (which is a high soluble sulfate) is the main responsible for AFt formation in these conditions. Moreover, tetracalcium aluminoferrite has modified ye'elimite hydration as AFt was not precipitated, and ye'elimite has inhibited tetracalcium aluminoferrite hydration as it did not react after 20 hours of hydration.

Acknowledgements

This work has been supported by Junta de Andalucía through P11-FQM-7517 research grant, by Spanish MINECO through MAT2010-16213 research grant, which is co-funded by FEDER and FEDER/University of Málaga (FC14-MAT-23) grant. We also thank CELLS-ALBA (Barcelona, Spain) for providing synchrotron beam time at BL04-MSPD beamline.

References

[1] Merlini M, Artioli G, Meneghini C, Cerulli T, Bravo A, Cella F. The early hydration and the set of Portland cements: In situ X-ray powder diffraction studies. Powder Diffr 2007; 22:201-208.

[2] Snellings R, Mertens G, Adriaens R, Elsen J. In situ synchrotron X-ray powder diffraction study of the early age hydration of cements blended with zeolite and quartzite fines and water-reducing agent. J Appl Clay Sci 2013; 72:124-131.

[3] Álvarez-Pinazo G, Cuesta A, García-Maté M, Santacruz I, Losilla ER, De la Torre AG, León-Reina L, Aranda MAG. Rietveld quantitative phase analysis of Yeelimite-containing cements. Cem Concr Res 2012; 42:960-971.

[4] De la Torre AG, Cabeza A, Calvente A, Bruque S, Aranda MAG. Full phase analysis of Portland clinker by penetrating synchrotron powder diffraction. Anal Chem 2001; 73:151-156.

[5] De la Torre AG, Aranda MAG. Accuracy in Rietveld quantitative phase analysis of Portland cements. J Appl Cryst 2013; 36:1169-1176.

[6] León-Reina L, De la Torre AG, Porras-Vázquez JM, Cruz M, Ordonez LM, Alcobe X, Gispert-Guirado F, Larrañaga-Varga A, Paul M, Fuellmann T, Schmidt R, Aranda MAG. Round robin on Rietveld quantitative phase analysis of Portland cements. J Appl Cryst 2009; 42:906-916.

[7] Scrivener KL, Füllmann T, Gallucci E, Walenta G, Bermejo E. Quantitative study of Portland cement hydration by X-ray diffraction/Rietveld analysis and independent methods. Cem Concr Res 2004; 34:1541-1547.

[8] Klaus SR, Neubauer J, Goetz-Neunhoeffer F. Hydration kinetics of CA_2 and CA - Investigations performed on a synthetic calcium aluminate cement. Cem Concr Res 2013; 43:62-69.

[9] Jansen D, Goetz-Neunhoeffer F, Stabler C, Neubauer J. A remastered external standard method applied to the quantification of early OPC hydration. Cem Concr Res 2011; 41:602-608.

[10] Clark SM, Barnes P. A comparison of laboratory, synchrotron and neutron diffraction for the real time study of cement hydration. Cem Concr Res 1995; 25:639-646.

[11] Aranda MAG, De la Torre AG, León-Reina L. Rietveld Quantitative Phase Analysis of OPC Clinkers, Cements and Hydration Products. Rev Mineral Geochem 2012; 74:169-209.

[12] Álvarez-Pinazo G, Cuesta A, García-Maté M, Santacruz I, Losilla ER, Ordóñez LM, Sanfélix S G, Fauth F, Aranda MAG, De la Torre AG. In-situ early-age hydration study of sulfobelite cements by synchrotron powder diffraction. Cem Concr Res 2014; 56:12-19.

[13] Cuesta A, Álvarez-Pinazo G, Sanfélix SG, Peral I, Aranda MAG, De la Torre AG. Hydration mechanisms of two polymorphs of synthetic ye'elimite. Cem Concr Res 2014; 63:127-136.

[14] Álvarez-Pinazo G, Santacruz I, León-Reina L, Aranda MAG, De la Torre AG. Hydration Reactions and Mechanical Strenght Developmenrts of Iron Rich Sulfobelite Eco-cements. Ind Eng Chem Res 2013; 52:16606-16614.

[15] Senff L, Castela A, Hajjaji W, Hotza D, Labrincha JA. Formulations of sulfobelite cement through design of experiments. Constr Build Mater 2011; 25:3410-3416.

[16] Bertaut EF, Blum P, Sagniers A. Structure du ferrite bicalcique et de la brownmillerite, Acta Crystallogr 1959; B12:149-159.

[17] Colville AA, Geller S. The crystal structure of brownmillerite, CA_2FeAlO_5. Acta Crystallogr 1971; B27:2311-2315.

[18] Colville AA, Geller S. The structures of $Ca_2Fe_{1.43}Al_{0.57}O_5$ and $Ca_2Fe_{1.28}Al_{0.72}O_5$. Acta Crystallogr 1972; B28:3196-3200.

[19] Touzo B, Scrivener KL, Glasser FP. Phase compositions and equilibria in the CaO-Al_2O_3-Fe_2O_3-SO_3 system, for assemblages containing ye'elimite and ferrite $Ca_2(Al,Fe)O_5$. Cem Concr Res 2013; 54:77-86.

[20] Redhammer GJ, Tippelt G, Roth G, Amthauer G. Structural variations in the brownmillerite series $Ca_2(Fe_{2-x}Al_x)O_5$: Single-crystal X-ray diffraction at 25ºC and high-temperature X-ray powder diffraction (25ºC ≤ T ≤ 1000ºC). Am Mineral 2004; 89:405-420.

[21] Taylor HFW. Cement Chemistry. London: Telford; 1997.

[22] Jupe AC, Turrillas X, Barnes P, Colston SL, Hall C, Hausermann D, Handfland M. Fast in situ x-ray-diffraction studies of chemical reactions: A synchrotron view of the hydration of tricalcium aluminate. Phys Rev 1996; B 53:14697-14700.

[23] Meredith P, Donald AM, Meller N, Hall C. Tricalcium aluminate hydration: Microstructural observations by in-situ electron microscopy. J Mater Sci 2004; 39:997-1005.

[24] Zivica V, Palou M, Bagel L, Krizma M. Low-Porosity tricalcium aluminate hardened paste. Constr Build Mater 2013; 38:1191-1198.

[25] Rogers DE, Aldridge LP. Hydrates of calcium ferrites and calcium aluminoferrites. Cem Concr Res 1977;7:399-410.

[26] Fukuhara M, Goto S, Asage K, Daimon M, Kondo R. Mechanisms and kinetics of C_4AF hydration with gypsum. Cem Concr Res 1981; 11:407–414.

[27] Odler I. In: Lea's chemistry of cement & concrete, ed. P. C. Hewlett, Butterworth-Heinemann, Oxford; 1998, p. 195–240.

[28] Meller N, Hall C, Jupe AC, Colston SL, Jacques SDM, Barnes P, Phipps J. The paste hydration of brownmillertire with and without gypsum: a time resolved synchrotron diffraction study at 30, 70, 100 and 150 ºC. J Mat Chem 2004; 14:428-435.

[29] Ectors D, Neubauer J, Goetz-Neunhoeffer F. The hydration of synthetic brownmillerite in presence of low Ca-sulfate content and calcite monitored by quantitative in-situ-XRD and heat flow calorimetry. Cem Concr Res 2013; 54:61-68.

[30] Dilnesa BZ, Lothenbach B, Renaudin G, Wichser A, Kulik D. Synthesis and characterization of hydrogarnet $Ca_3(Al_xFe_{1-x})_2(SiO_4)_y(OH)_{4(3-y)}$. Cem Concr Res 2014; 59:96-111.

[31] Flinp EP, McMurdie HF, Wells LS. Hydrothermal and X-ray studies of the garnet-hydrogarnet series and relationship of the series to hydration products of Portland cement. J Res Nat Bur Stand 1941; 26:13-33.

[32] Meller N, Hall C, Crawshaw J. ESEM evidence for through-solution transport during brownmillerite hydration. J Mat Sci 2004; 39:6611-6614.

[33] Cuesta A, De la Torre AG, Losilla ER, Peterson VK, Rejmak P, Ayuela A, Frontera C, Aranda MAG. Structure, atomistic simulations, and phase transition of stoichiometric ye`elimite. Chem Mater 2013; 25:1680-1687.

[34] Cuesta A, De la Torre AG, Losilla ER, Santacruz I, Aranda MAG. Pseudocubic Crystal Structure and Phase Transition in Doped Ye'elimite. Cryst Growth Des 2014; 14:5158-5163.

[35] De la Torre AG, Bruque S, Aranda MAG. Rietveld quantitative amorphous content analysis. J Appl Crystallogr 2001; 34:196-202.

[36] Jansen D, Stabler CH, Goetz-Neunhoeffer F, Dittrich S, Neubauer J. Does ordinary Portland cement contain amorphous phase? A quantitative study using an external standard method. Powder Diffrn 2011; 26:31-38.

[37] Fauth F, Peral I, Popescu C, Knapp M. The new Material Science Powder Diffraction beamline at ALBA Synchrotron. Powder Diffr 2013; 28:S360-S370.

[38] Larson AC, Von Dreele RB. General Structure Analysis System (GSAS). Los Alamos National Laboratory Report LAUR 2000; pp 86-748.

[39] Thompson P, Cox DE, Hasting JB. Rietveld refinement of Debye-Scherrer synchrotron X-ray data from Al_2O_3. J Appl Cryst 1987; 20:79-83.

[40] Larger GA, Armbruster TH, Faber J. Neutron and X-ray diffraction study of hydrogarnet $Ca_3Al_2(O_4H_4)_3$. A Miner 1987; 72:756-765.

[41] Winnefeld F, Barlag S. Calorimetric and thermogravimetric study on the influence of calcium sulfate on the hydration of ye'elimite. J Therm Anal Calorim 2010; 101:949-957.

[42] Allmann R. Refinement of the hybrid layer structure $[Ca_2Al(OH)_6]^+ \cdot [1/2SO_4 \cdot 3H_2O]^-$. Neues Jahrb Mineral Monatsh 1977; 136-144.

[43] Song F, Yu Z, Yang F, Lu Y, Liu Y. Microstructure of amorphous aluminium hydroxide in belite-calcium sulfoaluminate cement. Cem Concr Res 2015; 71:1-6.

Figure Captions

Figure 1. SXRPD Rietveld plot for $C_3A_{0.845}F_{0.155}H_6$ (λ~0.62Å). Inset details the high-angle region. The tic marks are the allowed Bragg reflections: $C_3A_{0.845}F_{0.155}H_6$ lower row; Quartz (internal standard) upper row.

Figure 2. Selected range of the SXRPD raw patterns for *$C_4AF\_g\_1.0$* recorded at different time of hydration, with the main peaks due to a given phase labelled; AFt: circle, AFm: star, Qz: triangle; $C\bar{S}H_2$: rhombus and C_4AF: inverted triangle.

Figure 3. Fe/Ca atomic ratio vs. Al/Ca atomic ratio for SEM-EDS study of a) *$C_4AF\_g\_1.0$*, b) *C_4AF_st-$C_4A_3\bar{S}\_g\_1.0$* (plus symbol) and *C_4AF_ss-$C_4A_3\bar{S}\_g\_1.0$* (crosses) at 48 hours. Solid symbols represent the theoretical composition of the phases: AFt: circle, AFm: star, C_4AF: inverted triangle and *$C_4A_3\bar{S}$*: square. SEM photograph of *$C_4AF\_g\_1.0$* (top) and *C_4AF_st-$C_4A_3\bar{S}\_g\_1.0$* (bottom).

Figure 4. Selected range of the SXRPD raw patterns for a) *C_4AF_st-$C_4A_3\bar{S}\_g\_1.0$* and b) *C_4AF_ss-$C_4A_3\bar{S}\_g\_1.0$* recorded at different hours of hydration, with the main peaks due to a given phase labelled as in Figure 2. The long arrow highlights one peak of C_4AF.

Figure 5. Full quantitative phase analysis results with time for a) *C_4AF_st-$C_4A_3\bar{S}\_g\_1.0$* and b) *C_4AF_ss-$C_4A_3\bar{S}\_g\_1.0$ ($C_4A_3\bar{S}$: square, $C\bar{S}H_2$: rhombus, C_4AF: inverted triangle, AFt: circle, AFm: star and ACn+FW: open square)*. Calorimetric heat flow curves (dashed line) are also displayed.

Figure 6. SXRPD Rietveld plots for a) *C_4AF_st-$C_4A_3\bar{S}\_g\_0.7$* and b) *C_4AF_st-$C_4A_3\bar{S}\_g\_1.3$*, at 12 hours of hydration, with the main peaks due to a given phase labelled as in Figure 2. Insets detail the low-angle regions.

Table 1. Paste mix proportions in weight percentages (wt%). The total heat evolved at 2 days of hydration is also given.

Mixture	C_4AF wt%	st-$C_4A_3\bar{S}$ wt%	ss-$C_4A_3\bar{S}$ wt%	gypsum wt%	water/solid	Total heat (J/g)
C_4AF_0.8	100	-	-	-	0.8	-
C_4AF_g_1.0	65.3	-	-	34.7	1.0	382.4
C_4AF_st-$C_4A_3\bar{S}$_g_1.0	32.7	49.1	-	18.2	1.0	382.2
C_4AF_ss-$C_4A_3\bar{S}$_g_1.0	32.7	-	49.1	18.2	1.0	409.1
C_4AF_st-$C_4A_3\bar{S}$_g_0.7	32.7	49.1	-	18.2	0.7	-
C_4AF_st-$C_4A_3\bar{S}$_g_1.3	32.7	49.1	-	18.2	1.3	-
C_4AF_st-$C_4A_3\bar{S}$_1.0	66.6	33.4	-	-	1.0	-

Table 2. Quantitative phase analysis results (wt%) for *C_4AF_0.8* paste, as a function of hydration time obtained by SXRPD. R_{WP} (%) disagreement factors are also given.

Wt%	t_o	1 h	2 h	3.5 h	5.5 h
C_4AF	46.5(1)	34.9(1)	32.1(1)	28.7(1)	24.9(1)
C_2AH_8	0	2.4(2)	1.5(3)	1.2(4)	1.4(5)
$C_3(A,F)H_6$	0	9.2(2)	14.7(2)	19.6(1)	24.8(1)
ACn+FW	9.1(1)+44.4*=53.4	53.5(1)	51.7(1)	50.5(1)	48.9(1)
R_{WP} (%)	9.2	7.0	7.4	7.3	7.3

*Theoretical free water content

Table 3. Elemental chemical composition (atomic wt%) of $C_3(A,F)H_6$ obtained by Rietveld methodology and transmission electron microscopy.

Element	Rietveld (wt%)	TEM (wt%)
Ca	65.7(-)	62(2)
Al	24.9(1)	21(2)
Fe	9.4(3)	17(3)

Table 4. Quantitative phase analysis results (wt%) for *C_4AF_g_1.0* paste, as a function of hydration time obtained by SXRPD. R_{WP} (%) disagreement factors are also given.

Wt%	t_o	5.5 h	12 h	16 h	18 h	21 h	29 h	48 h
C_4AF	29.7(1)	21.4(1)	19.1(1)	10.4(2)	7.7(3)	4.3(3)	2.6(4)	1.3(3)
$C\bar{S}H_2$	14.5(1)	5.6(1)	0.9(1)	0	0	0	0	0
AFt	0	23.6(1)	31.4(1)	25.5(2)	22.1(3)	19.1(4)	15.9(5)	15.5(5)
AFm	0	0	0	10.5(3)	14.4(4)	20.5(5)	20.0(6)	21.2(6)
ACn+FW	5.8(1)+50*=55.8	49.4(1)	48.5(1)	53.6(2)	55.8(2)	56.1(3)	61.4(3)	62.0(3)
R_{WP} (%)	7.0	5.7	5.4	10.8	9.7	13.8	14.3	13.2

*Theoretical free water content

Table 5. Quantitative phase analysis results (wt%) for *C_4AF_st-$C_4A_3\bar{S}$_g_0.7* paste, as a function of hydration time obtained by SXRPD. R_{WP} (%) disagreement factors are also given.

	t_o	1 h	4 h	6.5 h	12 h
$C_4A_3\bar{S}$	25.7(1)	23.7(1)	8.9(1)	7.9(1)	7.7(1)
$C\bar{S}H_2$	9.4(1)	9.8(1)	1.3(1)	1.2(1)	1.4(1)
C_4AF	16.4(1)	16.9(1)	15.2(1)	12.6(1)	11.3(1)
AFt	0	4.6(1)	28.9(1)	29.1(1)	27.6(1)
AFm	0	0	2.9(1)	3.7(2)	5.2(2)
ACn+FW	7.3(1)+41.2*=48.5	45.0(1)	42.7(1)	45.5(1)	46.8(1)
R_{WP} (%)	6.0	5.3	4.5	4.5	5.4

*Theoretical free water content

Table 6. Quantitative phase analysis results (wt%) for *C_4AF_st-$C_4A_3\bar{S}$_g_1.3* paste, as a function of hydration time obtained by SXRPD. R_{WP} (%) disagreement factors are also given.

	t_o	1 h	3.5 h	6.5 h	8.5 h	12 h
$C_4A_3\bar{S}$	19.1(1)	18.2(1)	5.2(1)	4.8(2)	5.0(2)	4.6(2)
$C\bar{S}H_2$	7.0(1)	6.3(1)	0.4(1)	0	0	0
C_4AF	12.2(1)	12.8(1)	9.1(1)	6.6(2)	5.4(2)	3.8(2)
AFt	0	3.2(1)	21.9(1)	19.5(2)	18.1(2)	15.2(2)
AFm	0	0	2.9(1)	6.4(2)	8.8(2)	11.8(2)
ACn+FW	5.3(1)+56.5*=61.8	59.6(1)	60.6(1)	62.7(1)	62.7(1)	64.6(2)
R_{WP} (%)	6.0	3.6	4.9	5.6	6.6	8.4

*Theoretical free water content

Table 7. Quantitative phase analysis results (wt %) for *C_4AF_st-$C_4A_3\bar{S}$_1.0* paste, as a function of hydration time obtained by SXRPD. R_{WP} (%) disagreement factors are also given.

	t_o	5 h	18 h	20 h
$C_4A_3\bar{S}$	31.5(1)	29.5(1)	10.9(2)	10.7(3)
C_4AF	14.9(1)	14.0(1)	15.8(2)	14.8(2)
AFm	0	0	17.9(3)	18.1(3)
ACn+FW	3.6(1)+50.0*=53.6	56.5(1)	55.4(2)	56.5(2)
R_{WP} (%)	5.4	4.2	10.6	10.7

*Theoretical free water content

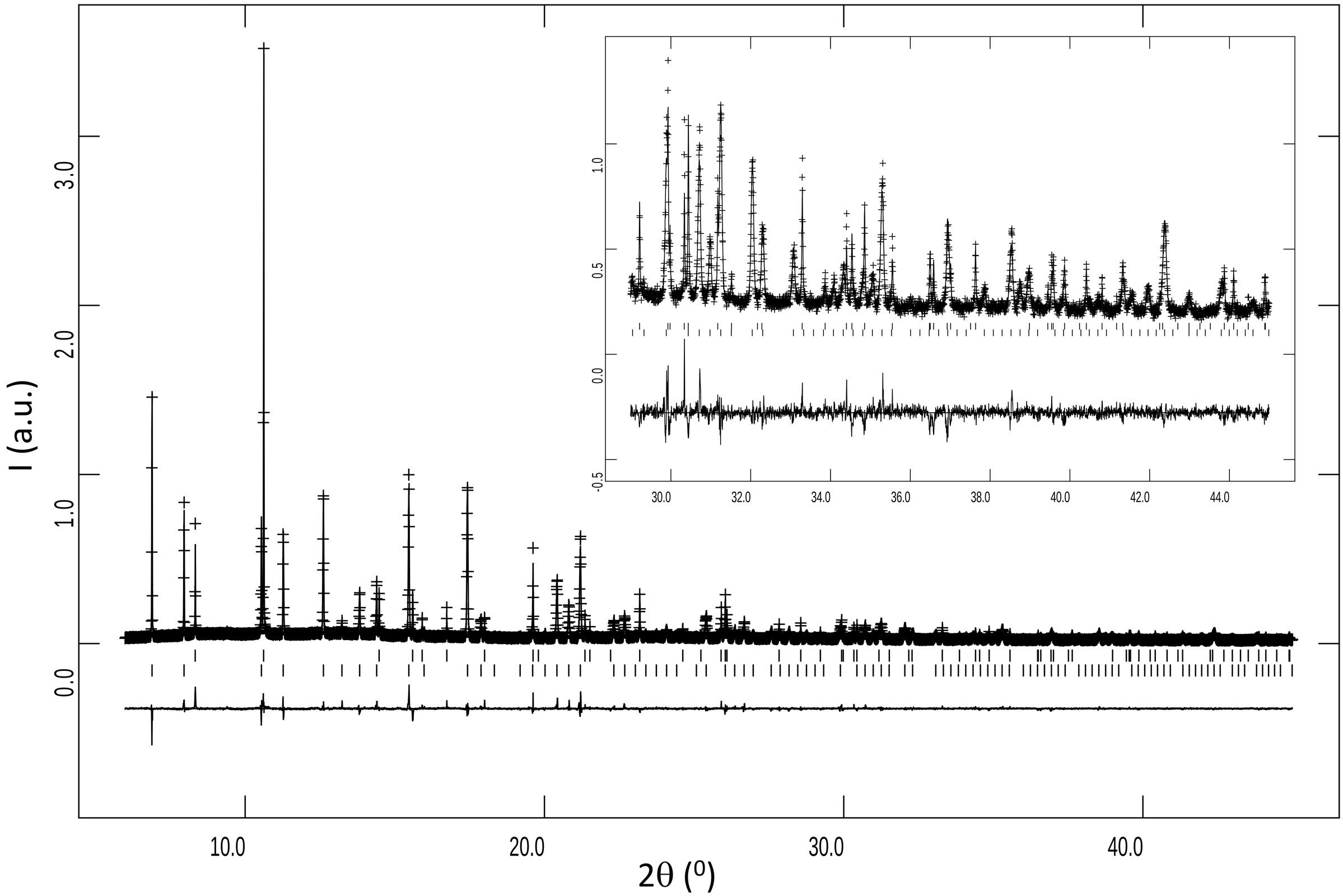
I (a.u.)
3.0
2.0
1.0
0.0
10.0
20.0
30.0
40.0
2θ (º)
1.0
0.5
0.0
-0.5
30.0
32.0
34.0
36.0
38.0
40.0
42.0
44.0

Figure 1

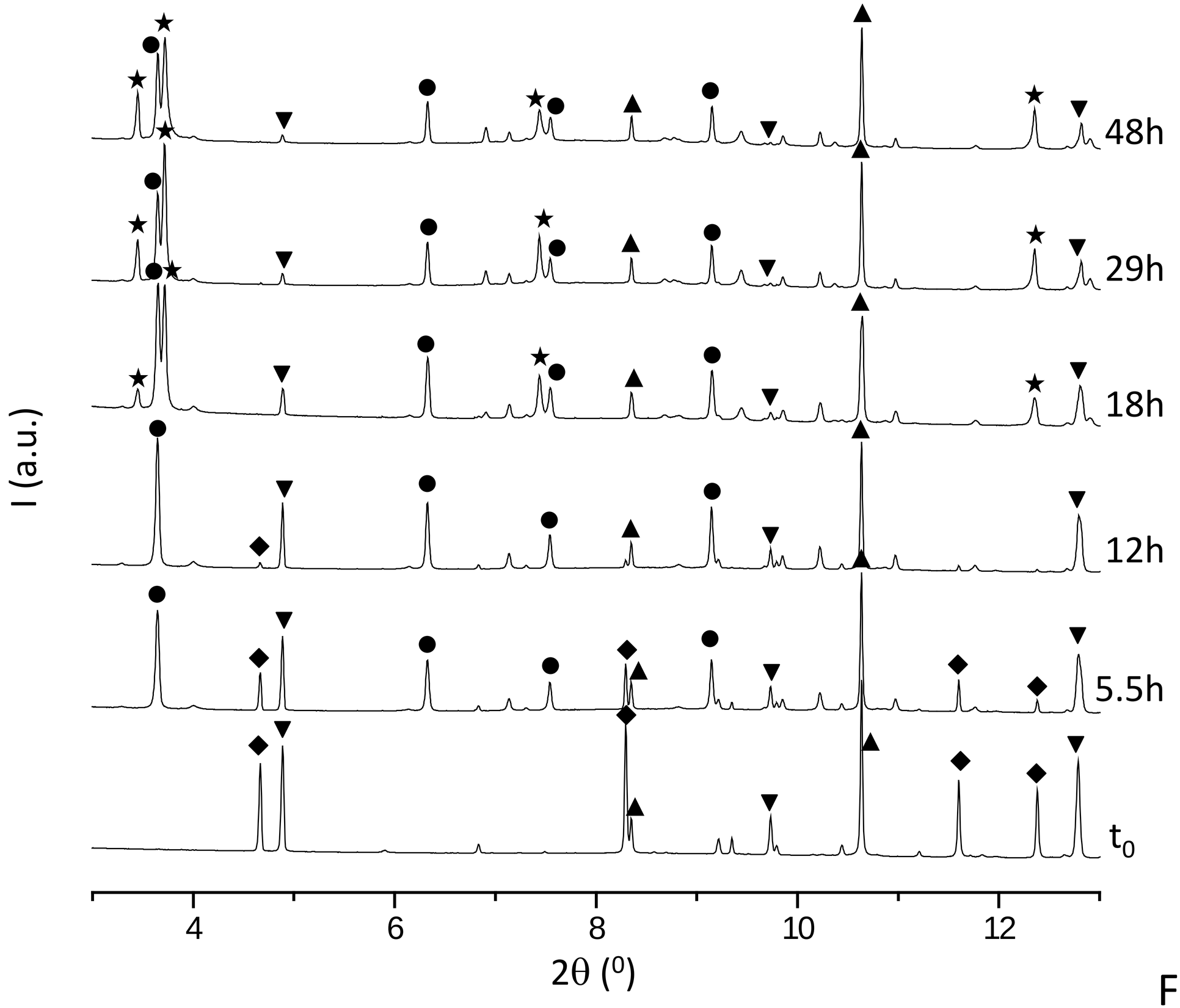

Figure 2

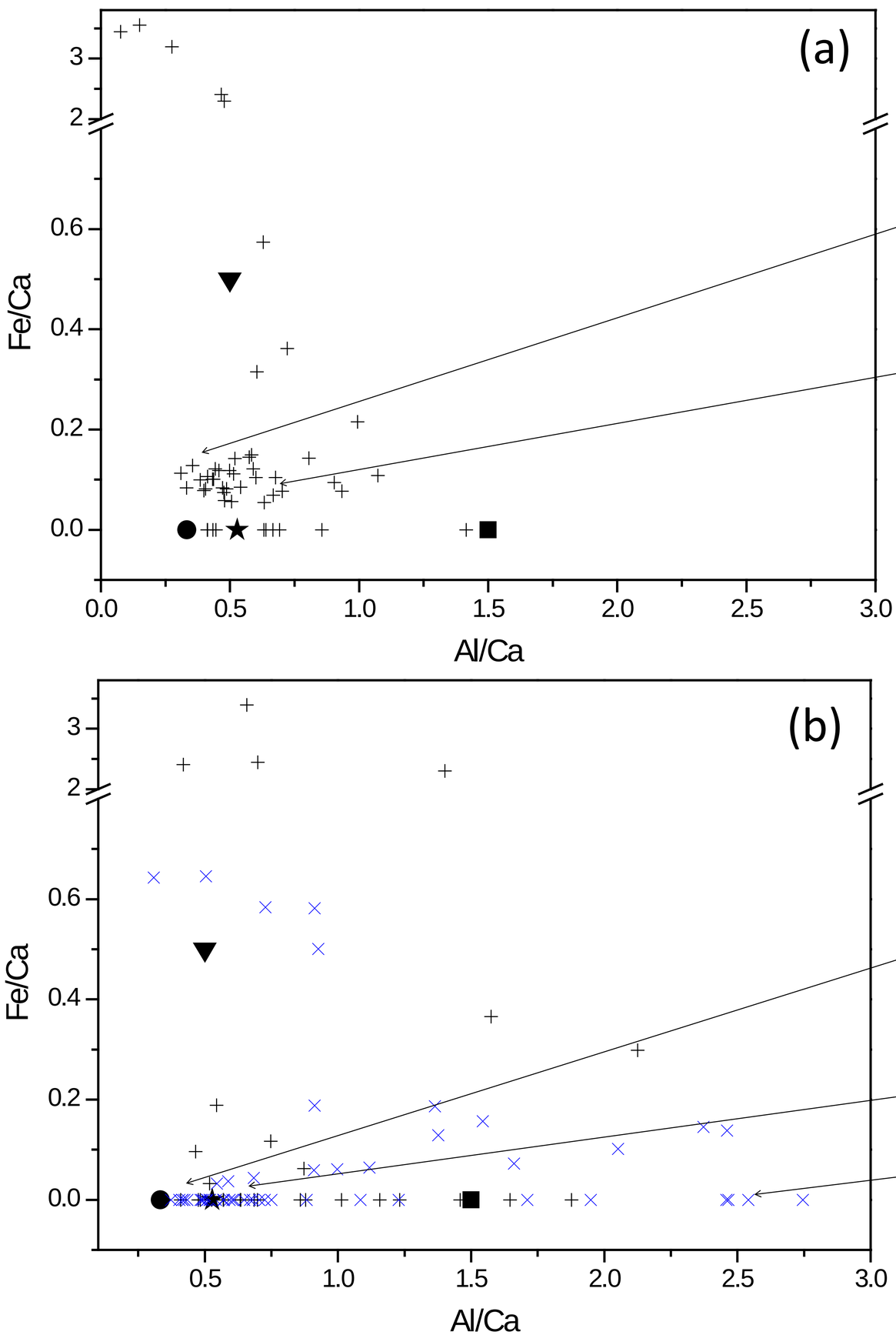
(a)
Fe/Ca
0.0
0.2
0.4
0.6
2
3
0.0
0.5
1.0
1.5
2.0
2.5
3.0
(b)
Al/Ca
Fe/Ca
Al/Ca

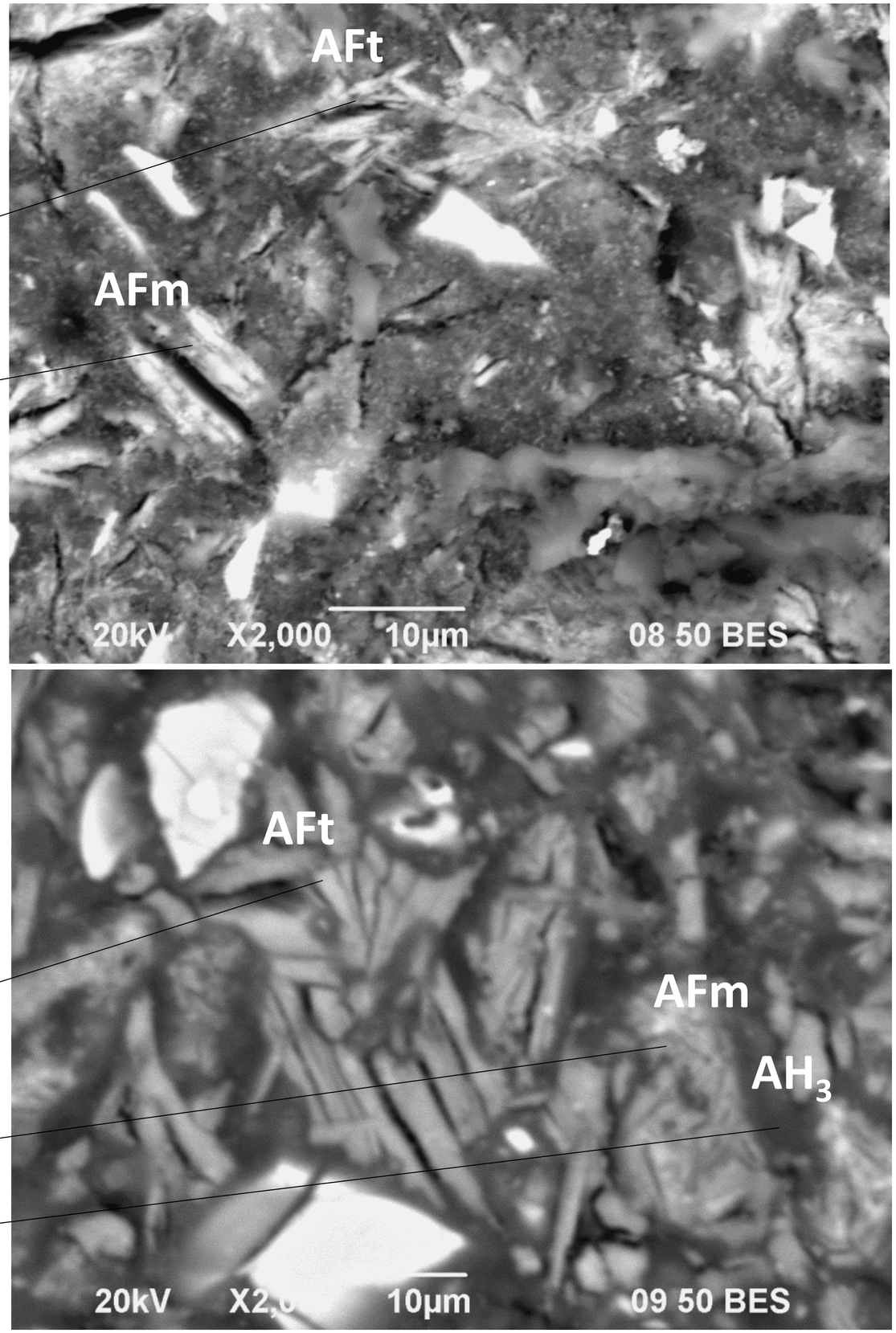
AFt
AFm
20kV X2,000 10µm 08 50 BES
AFt
AFm
AH3
20kV X2,0 10µm 09 50 BES

Figure 3

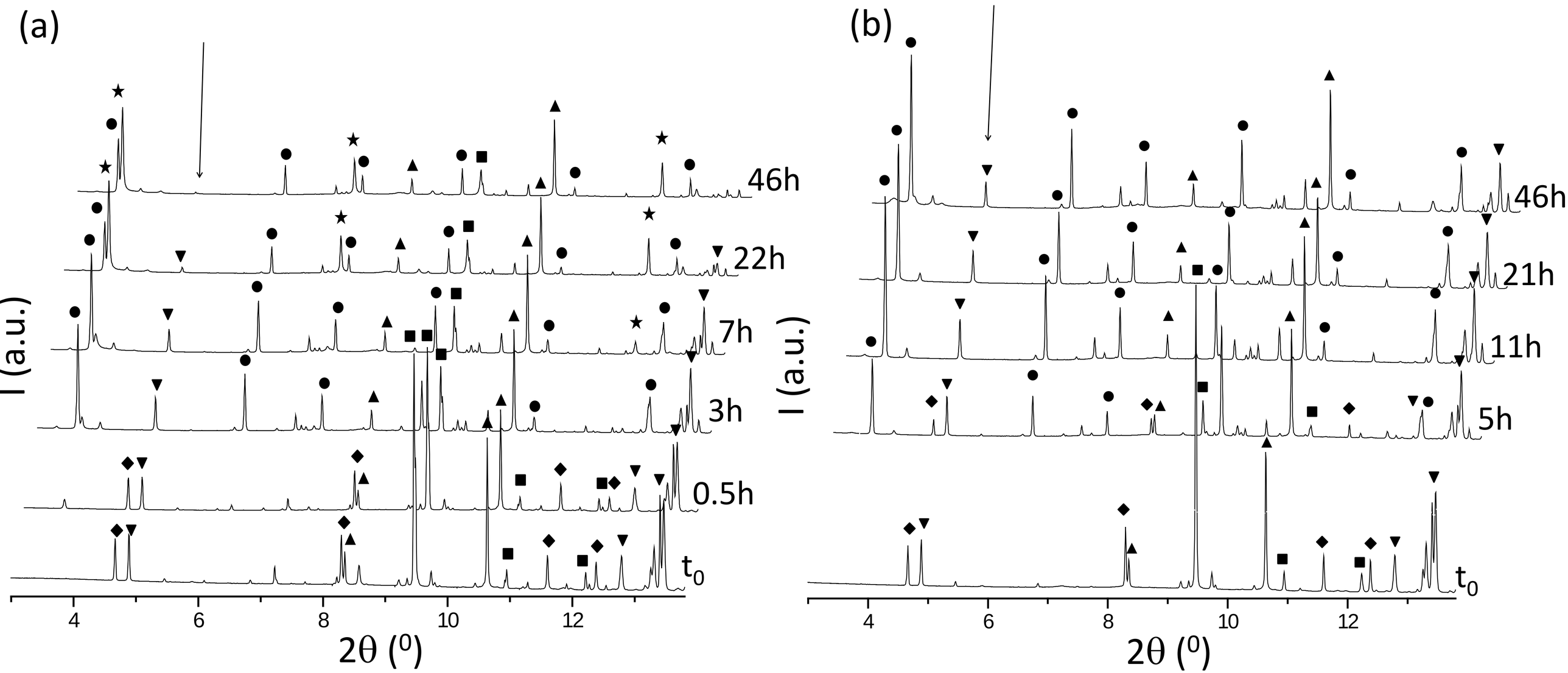

Figure 4

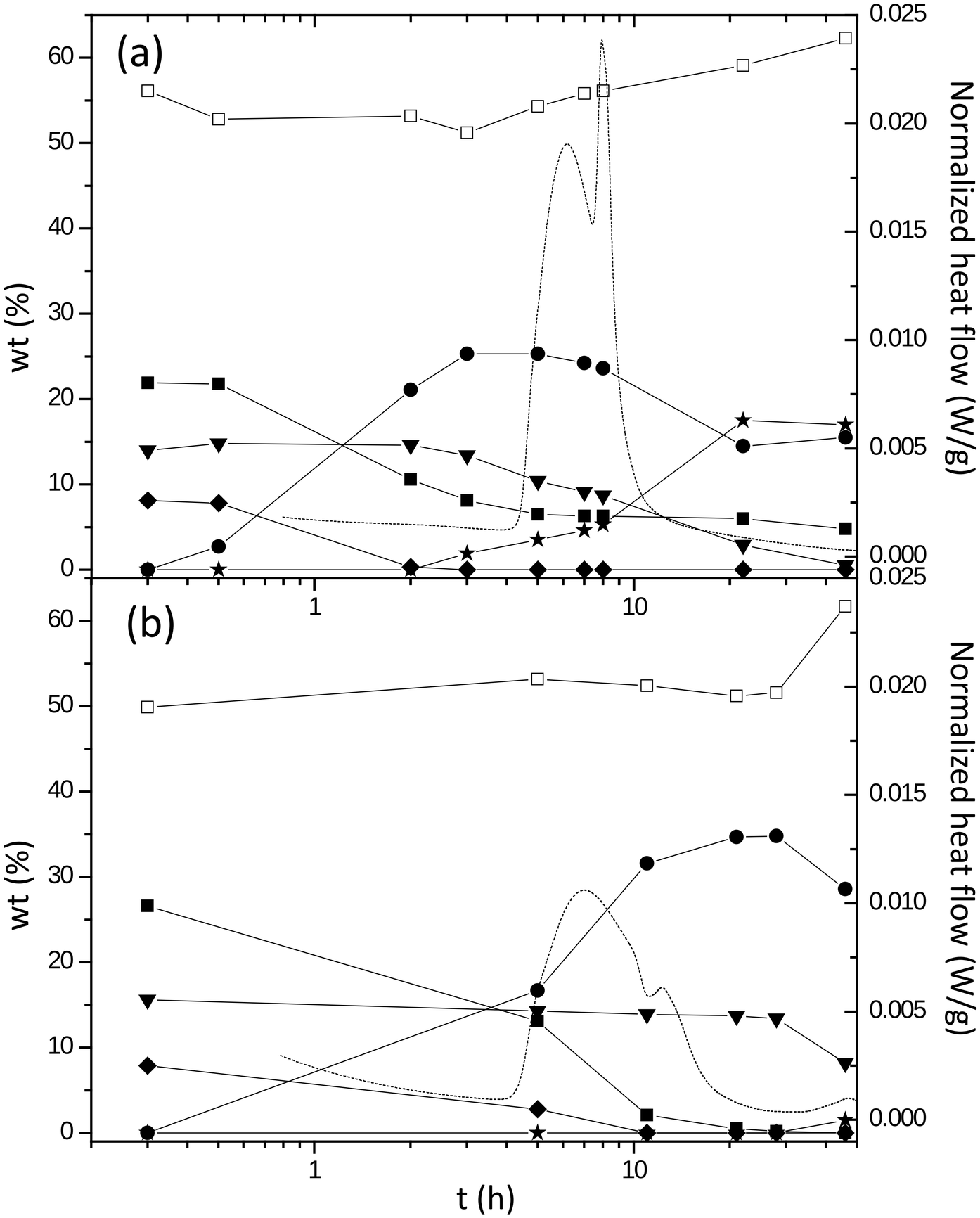
(a)
(b)
wt (%)
Normalized heat flow (W/g)
t (h)
0
10
20
30
40
50
60
1
10
0.000
0.005
0.010
0.015
0.020
0.025

Figure 5

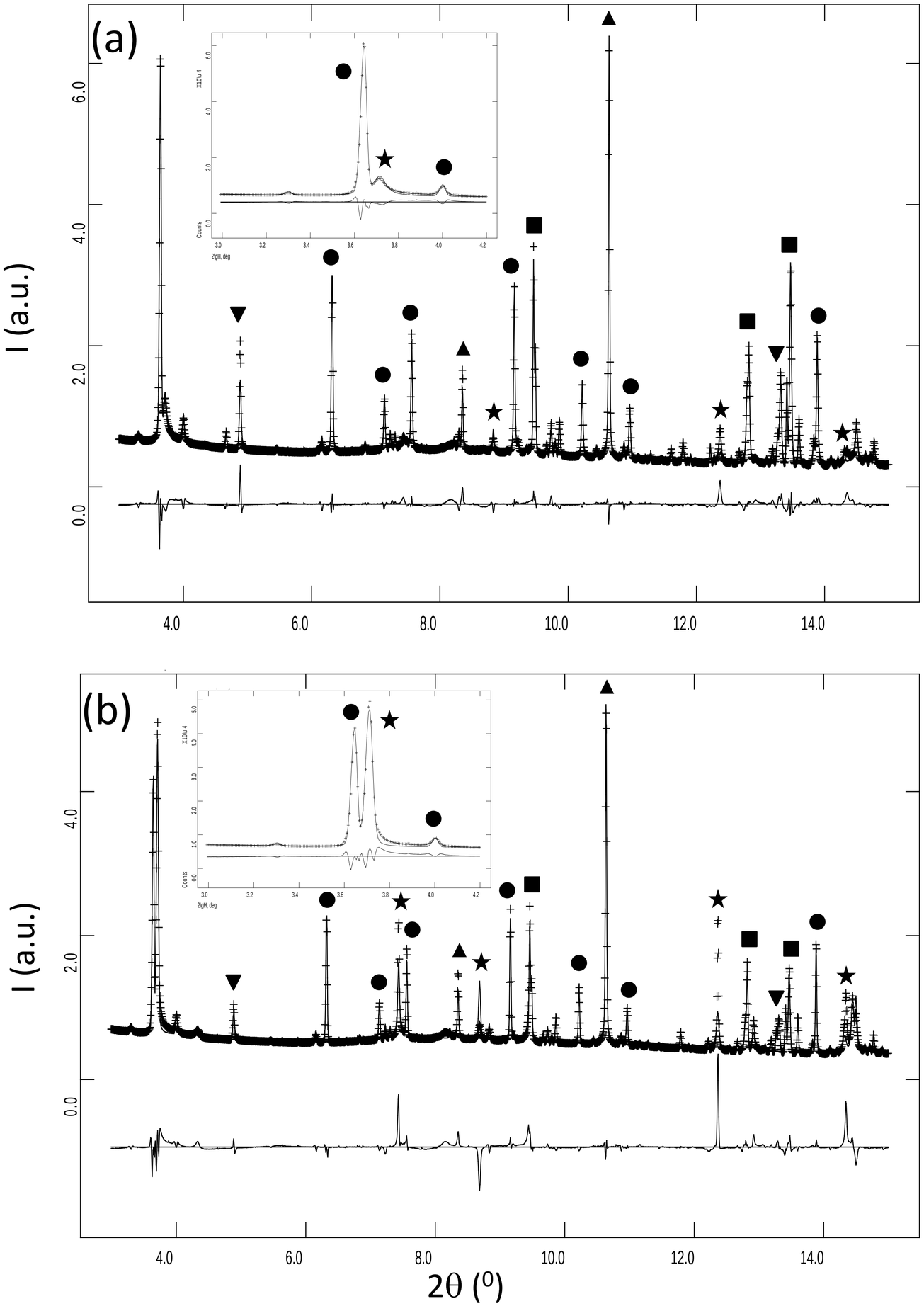
(a)
I (a.u.)
6.0
4.0
2.0
0.0
4.0
6.0
8.0
10.0
12.0
14.0
X10to 4
Counts
2tgH, deg
(b)
I (a.u.)
4.0
2.0
0.0
4.0
6.0
8.0
10.0
12.0
14.0
2θ (⁰)

Figure 6

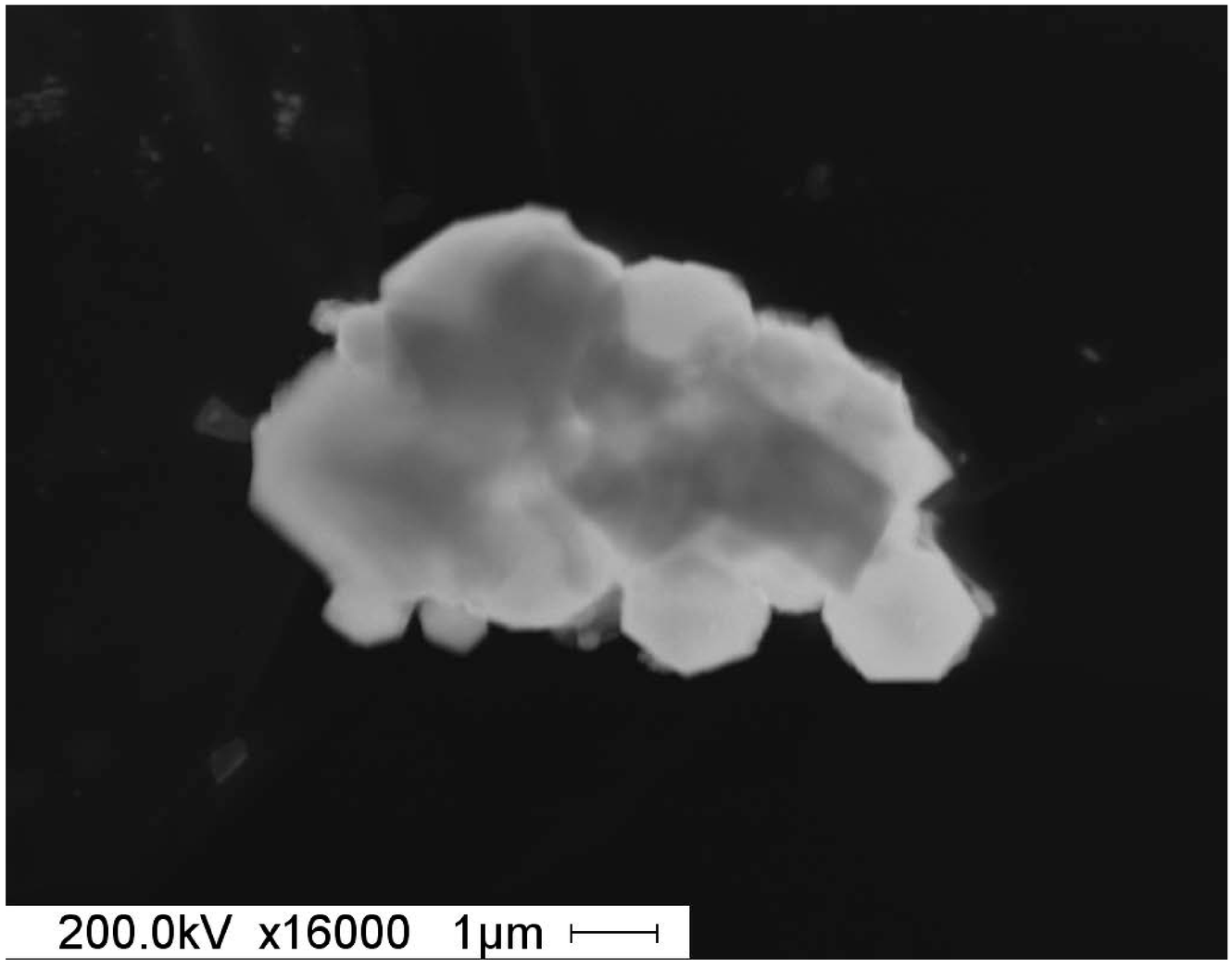

Figure S1

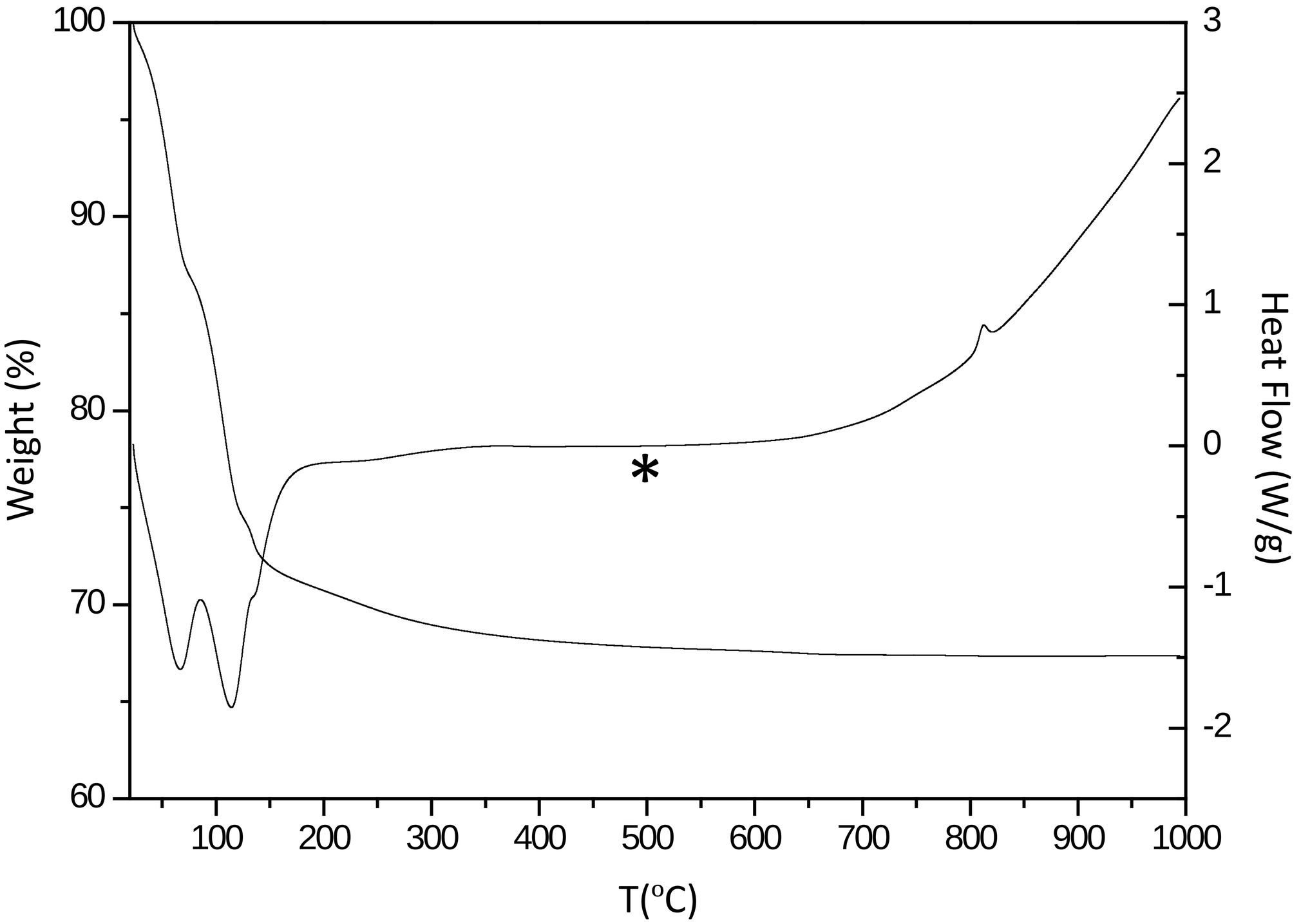
100
90
80
70
60
Weight (%)
3
2
1
0
-1
-2
Heat Flow (W/g)
100
200
300
400
500
600
700
800
900
1000
T(°C)
*

Figure S2

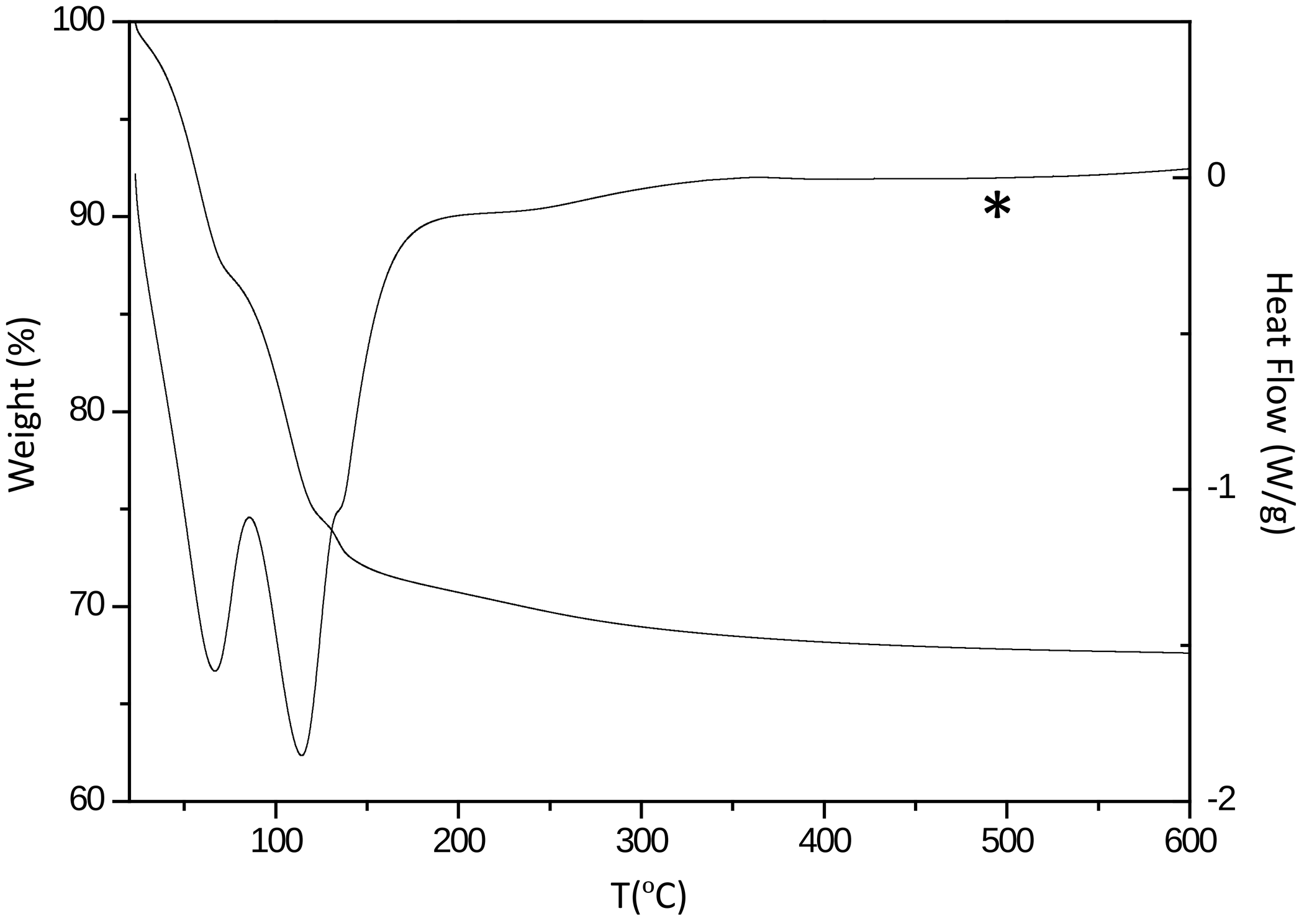
100
90
80
70
60
Weight (%)
0
-1
-2
Heat Flow (W/g)
*
100
200
300
400
500
600
T(°C)

Figure S2

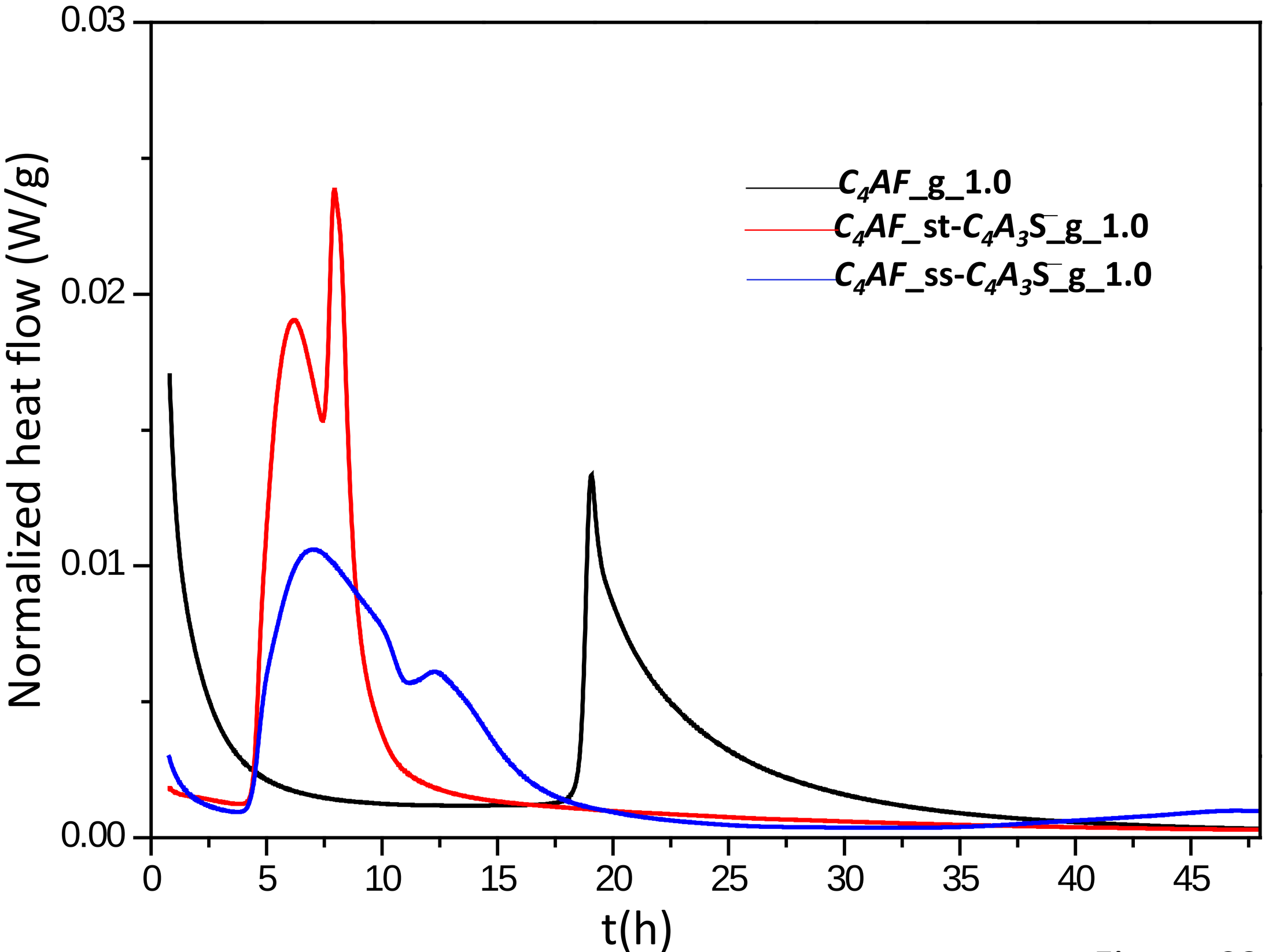
0.03
0.02
0.01
0.00
Normalized heat flow (W/g)
0
5
10
15
20
25
30
35
40
45
t(h)
C4AF_g_1.0
C4AF_st-C4A3S¯_g_1.0
C4AF_ss-C4A3S¯_g_1.0

Figure S3

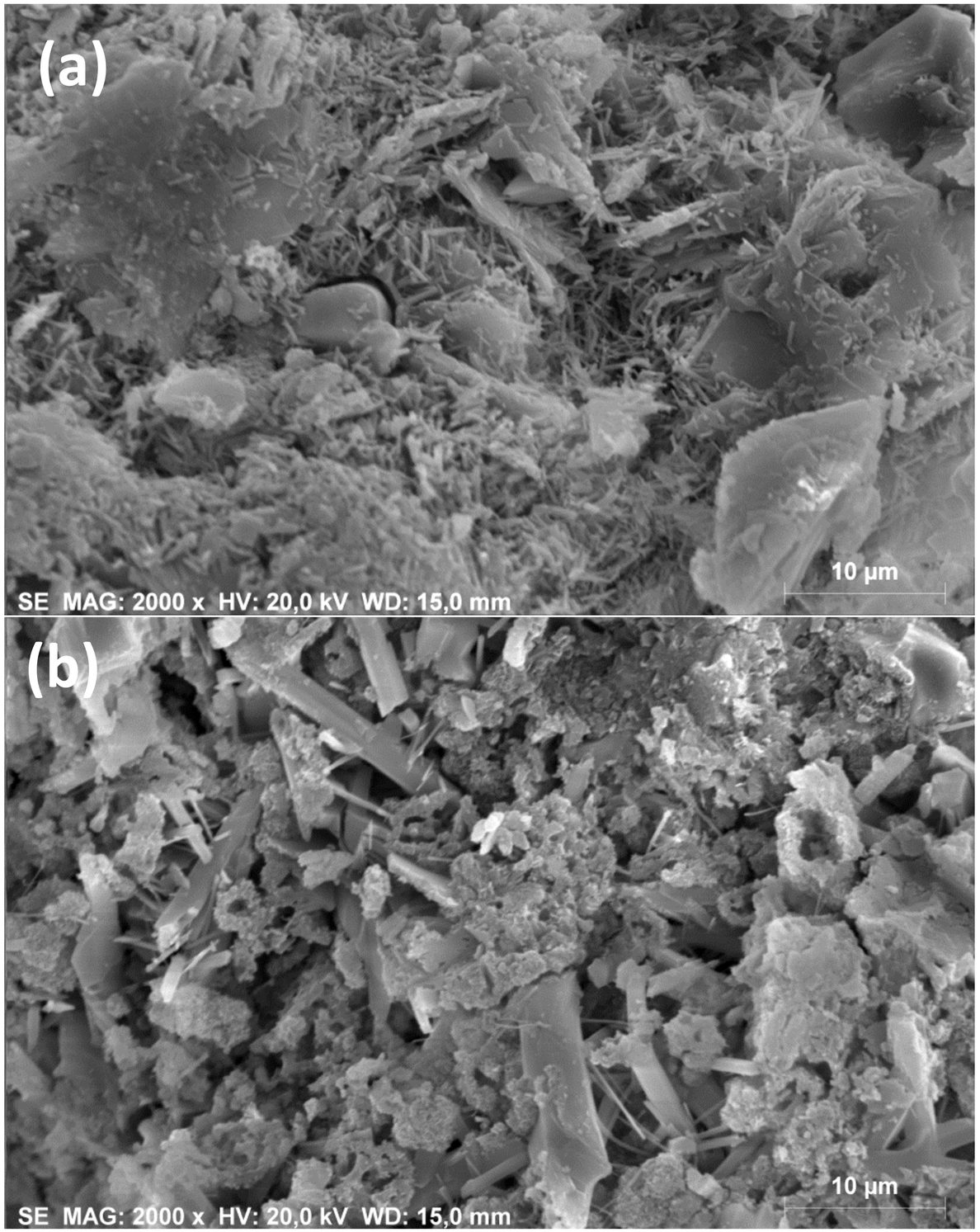
(a)
SE MAG: 2000 x HV: 20,0 kV WD: 15,0 mm
10 µm
(b)
SE MAG: 2000 x HV: 20,0 kV WD: 15,0 mm
10 µm

Figure S4

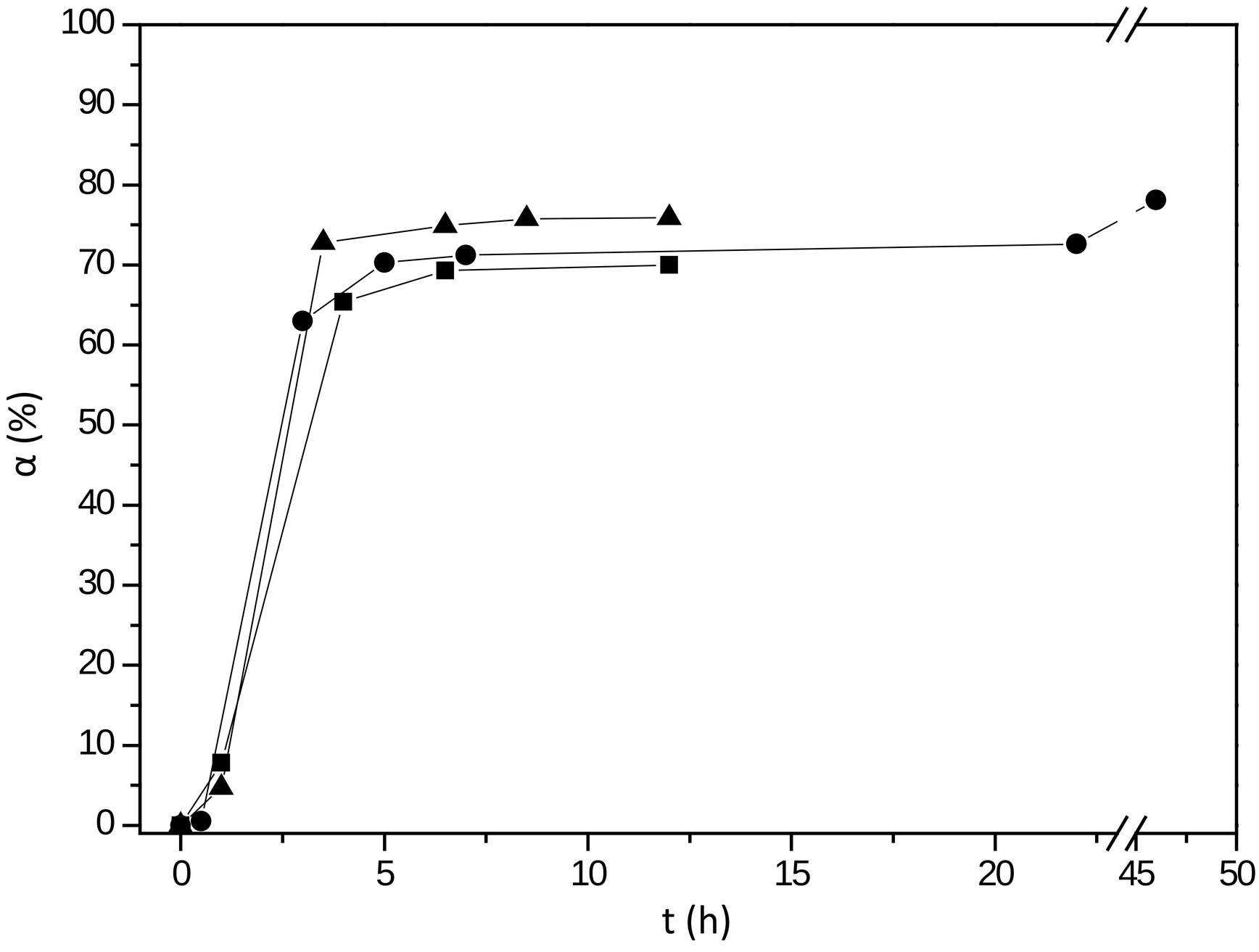

Figure S5